Acta Astronautica 104 (2014) 231–242

Contents lists available at ScienceDirect

Acta Astronautica

journal homepage: www.elsevier.com/locate/actaastro

Optimal diving maneuver strategy considering guidance accuracy for hypersonic vehicle

Jianwen Zhu [a], Luhua Liu [a], Guojian Tang [a,*], Weimin Bao [a,b]

[a] College of Aerospace Science and Engineering, National University of Defense Technology, Changsha 410073, China
[b] China Aerospace Science and Technology Corporation, Beijing 100048, China

ARTICLE INFO

Article history:
Received 27 December 2013
Received in revised form
20 May 2014
Accepted 21 July 2014
Available online 28 July 2014

Keywords:
Hypersonic vehicle
Dive phase
Three-dimensional guidance
Optimal control
Optimal maneuver strategy

ABSTRACT

An optimal maneuver strategy considering terminal guidance accuracy for hypersonic vehicle in dive phase is investigated in this paper. First, it derives the complete three-dimensional nonlinear coupled motion equation without any approximations based on diving relative motion relationship directly, and converts it into linear decoupled state space equation with the same relative degree by feedback linearization. Second, the diving guidance law is designed based on the decoupled equation to meet the terminal impact point and falling angle constraints. In order to further improve the interception capability, it constructs maneuver control model through adding maneuver control item to the guidance law. Then, an integrated performance index consisting of maximum line-of-sight angle rate and minimum energy consumption is designed, and optimal control is employed to obtain optimal maneuver strategy when the encounter time is determined and undetermined, respectively. Furthermore, the performance index and suboptimal strategy are reconstructed to deal with the control capability constraint and the serous influence on terminal guidance accuracy caused by maneuvering flight. Finally, the approach is tested using the Common Aero Vehicle-H model. Simulation results demonstrate that the proposed strategy can achieve high precision guidance and effective maneuver at the same time, and the indices are also optimized.

1. Introduction

Inspired by the excellent performance of hypersonic vehicle, such as flexible ballistic form and high lateral maneuver capability, much attention has been played on the corresponding research in recent years. As a popular research topic in aerospace field, the typical representation includes the American common aero vehicle (CAV) and Hypersonic Technology Vehicle 2 (HTV-2) which is considered as the expansion of CAV [1,2]. Dive phase is the last one in the whole flight phases, and the guidance is concerned with steering the vehicle to reach the designated termination target with prescribed accuracy. Due to the highly coupled, rapid varying, nonlinear motion model which contains large parametric uncertainties, the guidance which can satisfy multiple terminal constraints in presence of necessary path constraints and the maneuver penetration remain the key technical challenges [3]. Consequently, the diving maneuver strategy design considering the terminal guidance accuracy is more complicated and significant.

Most current researches focus on the guidance law derivation and maneuver model design separately. As for the high precision diving guidance, traditional algorithms

* Corresponding author.
E-mail address: gjtang@263.net (G. Tang).

http://dx.doi.org/10.1016/j.actaastro.2014.07.026
0094-5765/

simplify the three-dimensional (3D) diving motion into the two-dimensional planar motion, and derive the corresponding guidance law via advance control theories, such as optimal control [4,5] and sliding mode control [6]. However, despite the different control theories were fully employed, nearly all these guidance laws were deprived from zero line-of-sight (LOS) angle rate. Therefore, the trajectories were so straight forward that the penetrative ability will be greatly declined [7]. In order to improve maneuver performance, maneuvering flight, such as weaving and barrel roll maneuver can enhance penetrative ability effectively [8]. Great many factors can influence penetrative ability, in which the maneuver strategy is the most important one [9]. Actually, the diving maneuver penetration process is the mutual combat between pursuer and evader; therefore, both pursuit–evasion and differential game can be well adopted to obtain the optimal maneuver strategy, in which the perfect movement information for each other is needed [9–11]. As a result, the strategy will be much different if the movement information of pursuer cannot be determined completely. Using the limited ballistic parameters, Shinar gave the 3D maneuver control law [12]. Guo et al. discussed the maneuver control problem in ballistic middle phase with the assumption that the Kalman filter was used to predict the movement of evader and the evader adopts Singer maneuver model to increase prediction error, in which the H_∞ maneuver performance index is constructed with minimum energy consumption and maximum prediction error [13–16]. In addition, Ohlmeyer analyzed the influence on miss distance of sinusoidal maneuver, and presented an analytical expression of miss distance considering target initial-conditions uncertainties [17]. However, it is known that maneuvering flight can cause serious influence to the terminal guidance accuracy, and even lose the target [18]. Most current research about maneuvering flight focuses on maneuver model and strategy, ignoring the influence on guidance accuracy caused by maneuver, which means that it is necessary to construct the integrated performance index and design the novel maneuver strategy considering guidance accuracy.

Motivated by the aforementioned problems, a novel diving optimal maneuver strategy is considered in this paper, whose purpose is to obtain the optimal maneuver effect along with the high guidance accuracy at the same time. First, the complete nonlinear coupled relative motion equation, as the basis of the further research of guidance law and maneuver strategy, is constructed without any approximation. Second, with the help of feedback linearization and feedback control, the 3D guidance law which can satisfy multiple terminal constraints can be also obtained, and it is convenient to achieve maneuvering flight though adding maneuver control item into the original guidance law. Moreover, considering the difference when the encounter time is determined and undetermined, it will establish the optimal performance indices to evaluate the maneuver performance and design the maneuver strategies using optimal control for each case. In addition, combining the control capability limitation, especially the terminal guidance accuracy, the performance indices under different situations will be reconstructed, and then the optimal strategy and guaranteed cost maneuver strategy will be also obtained. Finally, the maneuver parameters can be optimized through several groups of simulations. The main contributions of this paper are the establishment of 3D relative motion equation, the construction of maneuver control equation, the design of the maneuver performance indices and optimal maneuver strategies, the reconstruction of indices and strategies that the terminal guidance accuracy and control capability are fully considered.

2. Problem formulation

2.1. Formulation of motion

The three-degree-of-freedom (3DOF) point-mass dynamic under ballistic coordinate system is adopted [4]. For hypersonic vehicle, owing to the high flight velocity, short flight time and low altitude in dive phase, compared with the aerodynamic force and gravity, the Carioles inertial force and centrifugal inertial force caused by the earth's self-rotation are very small, and the accelerations are approximately $10^{-2}g_0$ and $10^{-3}g_0$, respectively [4]. Therefore, the non-rotating spherical earth assumption is employed in the motion equation construction and guidance law design; the motion equations in ballistic coordinate system are given in the following Eq. (1):

$$\begin{cases} \dot{v} = -\dfrac{\rho v^2 S_m C_D}{2m} - g\ \sin\ \theta \\ \dot{\theta} = \dfrac{\rho v^2 S_m C_L\ \cos\ \upsilon}{2mv} - \dfrac{g\ \cos\ \theta}{v} + \dfrac{v\ \cos\ \theta}{r} \\ \dot{\sigma} = -\dfrac{\rho v^2 S_m C_L\ \sin\ \upsilon}{2mv\ \cos\ \theta} + \dfrac{v\ \tan\ \phi\ \cos\ \theta\ \sin\ \sigma}{r} \\ \dot{\varphi} = \dfrac{v\ \cos\ \theta\ \cos\ \sigma}{r} \\ \dot{\lambda} = -\dfrac{v\ \cos\ \theta\ \sin\ \sigma}{r\ \cos\ \phi} \\ \dot{r} = v\ \sin\ \theta \end{cases} \tag{1}$$

where the position coordinates are the radial distance from the center of the Earth to the vehicle r, the longitude λ, the latitude φ; and the velocity coordinates are the earth-relative velocity magnitude v, the velocity slope angle θ, and velocity azimuth angle σ measured from the north in a clockwise direction. ρ is the atmospheric density; m is the vehicle mass; S_m is the reference area; $g = \mu_M/r^2$ is the gravity; μ_M is the gravitational constant. C_D and C_L are the drag and lift coefficients, respectively, and both these aerodynamic coefficients are the function of the Mach number, altitude and angle of attack (sometimes independent of altitude, such as CAV-H [1]). In these coefficients, control variables include angle of attack α and the bank angle υ.

2.2. Relative motion equations

Traditional decoupled guidance needs to divide the diving motion into diving and turning sub-planes with the assumption that the three-dimensional diving motion can be decoupled into longitudinal and lateral directions [4]. However, due to high flight velocity, the coupling between longitudinal and lateral motions is very high, especially when large amplitude lateral maneuver is adopted. As a

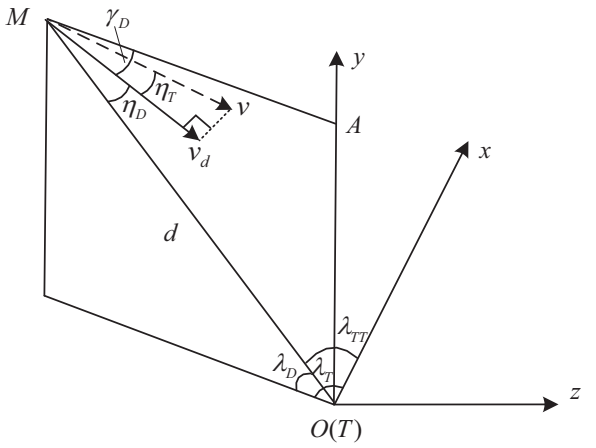

Fig. 1. Three-dimensional coupled relative motion.

result, as the basis of the further guidance and maneuver research, it is necessary to establish the 3D coupled relative motion equations to describe the diving motion clearly. To begin with, target coordinate system $O-xyz$ with the origin on the target, the x-axis pointing north, y-axis pointing upward, and z-axis pointing east is established and the relative motion relationship is shown in Fig. 1.

In Fig. 1, M and T refer to vehicle and target, respectively, $\overrightarrow{MA}$ is the parallel of current horizon. It is known that 3D diving motion can be described in longitudinal and lateral directions, where longitudinal motion can be described in the MAO plane and lateral channel can be determined by current velocity vector $\boldsymbol{v}$ and the component in the MAO plane $\boldsymbol{v}_d$. In addition, d is the sight distance between the vehicle and target, λ_D is the LOS elevation angle, γ_D is the longitudinal velocity azimuth defined as the included angle between $\overrightarrow{MA}$ and $\boldsymbol{v}_d$, η_D is the included angle between v_d and LOS, η_T is the included angle between $\boldsymbol{v}$ and $\boldsymbol{v}_d$, γ_T is the lateral velocity azimuth, and λ_{TT} is the LOS azimuth. Both γ_T and λ_{TT} are measured from the north in a clockwise direction. Then the following equations hold:

$$\begin{cases} \dot{d} = -v\cos\eta_T\cos\eta_D \\ d\dot{\lambda}_D = v\cos\eta_T\sin\eta_D \\ d\dot{\lambda}_{TT} = v\sin\eta_T\cos\eta_D \end{cases} \tag{2}$$

in which $\dot{d}$ is the rate of change of relative distance. Differentiation is performed on the second and third equations of Eq. (2):

$$\begin{cases} \dot{d}\dot{\lambda}_D + d\ddot{\lambda}_D = \dot{v}\cos\eta_T\sin\eta_D - v\dot{\eta}_T\sin\eta_T\sin\eta_D + v\dot{\eta}_D\cos\eta_T\cos\eta_D \\ \dot{d}\dot{\lambda}_{TT} + d\ddot{\lambda}_{TT} = \dot{v}\sin\eta_T\cos\eta_D + v\dot{\eta}_T\cos\eta_T\cos\eta_D - \dot{\eta}_D v\sin\eta_T\sin\eta_D \end{cases} \tag{3}$$

where $\dot{v}$ is the velocity magnitude differential. Substituting Eq. (2) into Eq. (3) will yield the following equations:

$$\begin{cases} \dot{d}\dot{\lambda}_D + d\ddot{\lambda}_D = \frac{\dot{v}}{v}d\dot{\lambda}_D - v\dot{\eta}_T\sin\eta_T\sin\eta_D - \dot{\eta}_D\dot{d} \\ \dot{d}\dot{\lambda}_{TT} + d\ddot{\lambda}_{TT} = \frac{\dot{v}}{v}d\dot{\lambda}_{TT} - v\dot{\eta}_D\sin\eta_T\sin\eta_D - \dot{\eta}_T\dot{d} \end{cases} \tag{4}$$

according to the geometry relationship:

$$\begin{cases} \eta_D = \lambda_D + \gamma_D \\ \eta_T = \lambda_{TT} - \gamma_T \end{cases} \tag{5}$$

then, Eq. (4) can be rewritten as

$$\begin{cases} \ddot{\lambda}_D = \left(\frac{\dot{v}}{v} - 2\frac{\dot{d}}{d}\right)\dot{\lambda}_D - \frac{v\sin\eta_T\sin\eta_D}{d}(\dot{\lambda}_{TT} - \dot{\gamma}_T) - \frac{\dot{d}}{d}\dot{\gamma}_D \\ \ddot{\lambda}_{TT} = \left(\frac{\dot{v}}{v} - 2\frac{\dot{d}}{d}\right)\dot{\lambda}_{TT} - \frac{v\sin\eta_T\sin\eta_D}{d}(\dot{\lambda}_D + \dot{\gamma}_D) + \frac{\dot{d}}{d}\dot{\gamma}_T \end{cases} \tag{6}$$

Comparing these equations with the decoupled equations based on the simplified planar motion [5], Eq. (6) adds the coupling factor between longitudinal and lateral motions; therefore, it can describe relative diving motion more accurately. Here, we define the coupling coefficient:

$$A_{DT} = \frac{v\sin\eta_T\sin\eta_D}{d} \tag{7}$$

It is evident that the coupling coefficient A_{DT} increases as η_D, η_T and velocity v increase, while decreases as the sight distance d increases. As a result, the coupling coefficient A_{DT} will be close to zero when η_D, η_T and v are small and the relative distance d is very large, which means the coupling equations can be the simplified into decoupled ones as shown in Ref. [4]. The velocity azimuth η_D and η_T can be calculated:

$$\begin{cases} \eta_T = \lambda_T - \sigma \\ \eta_D = \arccos(\dot{d}/v\cos\eta_T) \end{cases} \tag{8}$$

We can refer to Ref. [4] for more information and the computation of the relative motion coefficients $\lambda_D, \lambda_{TT}, \dot{\lambda}_D, \dot{\lambda}_{TT}, d, \dot{d}$. For diving guidance, the attack direction is free, regardless of the strict constraints for terminal impact point and falling angle. In order to take advantage of control method to resolve guidance problem, we begin with the introduction of state variables, control variables and output variables via motion Eq. (6):

$$\begin{cases} \boldsymbol{x} = [x_1, x_2]^T = [\dot{\lambda}_D + k(\lambda_D + \theta_f), \dot{\lambda}_{TT}]^T \\ \boldsymbol{u} = [u_1, u_2]^T = [\dot{\gamma}_D, \dot{\gamma}_T]^T \\ \boldsymbol{h}(\boldsymbol{x}) = [h_1(x), h_2(x)]^T = [\dot{\lambda}_D + k(\lambda_D + \theta_f), \dot{\lambda}_{TT}]^T \end{cases} \tag{9}$$

where θ_f is the required terminal impact angle, $k > 0$ is the revise coefficient for terminal angle. It is known that the guidance objective is to realize:

$$\begin{cases} \lim_{t\to t_f} x_1(t) = 0 \\ \lim_{t\to t_f} x_2(t) = 0 \end{cases} \tag{10}$$

denote $T_{go} = -d/\dot{d}$ as the flight time to go, then Eq. (6) can be rewritten as

$$\begin{cases} \dot{x}_1 = \left(\frac{\dot{v}}{v} + \frac{2}{T_{go}} + 1\right)(x_1 - k(\lambda_D + \theta_f)) - A_{DT}x_2 + A_{DT}\dot{\gamma}_T + \frac{1}{T_{go}}\dot{\gamma}_D \\ \dot{x}_2 = \left(\frac{\dot{v}}{v} + \frac{2}{T_{go}}\right)x_2 - A_{DT}(x_1 - k(\lambda_D + \theta_f)) - A_{DT}\dot{\gamma}_D - \frac{1}{T_{go}}\dot{\gamma}_T \end{cases} \tag{11}$$

The above equations can be expressed as the standard form of nonlinear control system:

$$\begin{cases} \dot{\boldsymbol{x}} = \boldsymbol{f}(\boldsymbol{x}) + \boldsymbol{g}(\boldsymbol{x})u \\ \boldsymbol{y} = \boldsymbol{h}(\boldsymbol{x}) \end{cases} \tag{12}$$

where

$$\mathbf{f}(\mathbf{x}) = \begin{bmatrix} \left(\frac{\dot{v}}{v} + \frac{2}{T_{go}} + 1\right)(x_1 - k(\lambda_D + \theta_f)) - A_{DT}x_2 \\ \left(\frac{\dot{v}}{v} + \frac{2}{T_{go}}\right)x_2 - A_{DT}(x_1 - k(\lambda_D + \theta_f)) \end{bmatrix},$$

$$\mathbf{g}(\mathbf{x}) = \begin{bmatrix} \frac{1}{T_{go}} & A_{DT} \\ -A_{DT} & -\frac{1}{T_{go}} \end{bmatrix} \tag{13}$$

3. 3D guidance law and maneuver control equations

According to the analysis in Section 1, the 3D high precision coupled guidance law design is still a key technical challenge for hypersonic vehicle. The diving guidance problem can be described as follows: given the initial condition of the vehicle, design guidance law to steer the vehicle to attack the ground fixed target under the flexible multiple path constraints, while satisfying the constraint of terminal impact angle and eliminating the position error. Because of the coupling and nonlinear characteristics of the diving motion described in Eq. (12), it is too difficult to design the guidance law directly. Therefore, we can employ feedback linearization to decouple and linearize the original nonlinear guidance equations, and then the design of the guidance law can be greatly simplified. Meanwhile, feedback control can be also used to design the guidance law. Finally, 3D diving guidance law is obtained through substituting the feedback control law of the linear equations into the original nonlinear system.

3.1. 3D guidance law

Given the nonlinear system Eq. (12) and the corresponding input and output state variables, if the system satisfies

(1) $L_{gj}L_f^k h_i(x) = 0, (1 \le i \le m, 1 \le j \le m, 1 \le k \le r_i - 1)$
(2) The $m \times m$ matrix:

$$\mathbf{P}(x) = \begin{bmatrix} L_{g1}L_f^{r_1-1}h_1(x) & \cdots & L_{gm}L_f^{r_1-1}h_1(x) \\ L_{g1}L_f^{r_2-1}h_2(x) & \cdots & L_{gm}L_f^{r_2-1}h_2(x) \\ \cdots & \cdots & \cdots \\ L_{g1}L_f^{r_m-1}h_m(x) & \cdots & L_{gm}L_f^{r_m-1}h_m(x) \end{bmatrix} \tag{14}$$

being nonsingular at $\mathbf{x} = \mathbf{x}_0$, then the system is said to have a relative degree $r = \Sigma_{i=1}^{m} r_i$, and it is linearizable if sufficiently smooth function $\mathbf{y} = \mathbf{h}(\mathbf{x})$ exists so that the relative degree of the system is $r = \Sigma_{i=1}^{m} r_i = n$ [19].

The relative degree of system Eq. (12) is $r = 2$, with $r_1 = r_2 = 1$, and the decoupled matrix:

$$\boldsymbol{P}(\boldsymbol{x}) = \begin{bmatrix} L_{g1}h_1(x) & L_{g2}h_1(x) \\ L_{g1}h_2(x) & L_{g2}h_2(x) \end{bmatrix} = \begin{bmatrix} \frac{1}{T_{go}} & A_{DT} \\ -A_{DT} & -\frac{1}{T_{go}} \end{bmatrix} \tag{15}$$

is nonsingular at the equilibrium state. Therefore, the nonlinear guidance system satisfies the condition in Eq. (14), which means it can be decoupled into linear equations with the same relative degree. The new state variables are

$$\boldsymbol{z} = \boldsymbol{T}(\boldsymbol{x}) = [h_1(x), h_2(x)]^T = [\lambda_D + k(\lambda_D + \theta_f), \dot{\lambda}_{TT}]^T \tag{16}$$

and the inputs transform:

$$\boldsymbol{u} = \boldsymbol{P}^{-1}(\boldsymbol{x})[-\boldsymbol{Q}(\boldsymbol{x}) + \boldsymbol{v}] \tag{17}$$

where $\boldsymbol{v} = [v_y, v_z]^T$ is the new control variable, and

$$\begin{aligned} \boldsymbol{Q}(\boldsymbol{x}) &= \begin{bmatrix} L_{\mathbf{f}}h_1(x) \\ L_{\mathbf{f}}h_2(x) \end{bmatrix} \\ &= \begin{bmatrix} \left(\frac{\dot{v}}{v} + \frac{2}{T_{go}} + 1\right)(x_1 - k(\lambda_D + \theta_f)) - A_{DT}x_2 \\ \left(\frac{\dot{v}}{v} + \frac{2}{T_{go}}\right)x_2 - A_{DT}(x_1 - k(\lambda_D + \theta_f)) \end{bmatrix} \end{aligned} \tag{18}$$

Combine Eqs. (15)–(18), we can get the linear decoupled system:

$$\begin{cases} \dot{\boldsymbol{z}} = A\boldsymbol{v} \\ \boldsymbol{y} = \boldsymbol{C}\boldsymbol{z} \end{cases} \tag{19}$$

where the new state matrix and output matrix are

$$\boldsymbol{A} = \begin{bmatrix} 1 & 0 \\ 0 & 1 \end{bmatrix}, \boldsymbol{C} = \begin{bmatrix} 1 & 0 \\ 0 & 1 \end{bmatrix} \tag{20}$$

In Eq. (20), both $\boldsymbol{A}$ and $\boldsymbol{C}$ are in the *Brunovsky* standard form with relevant rank [19], and it is obvious that the linear control system is controllable completely. With the linear equations expressed in Eq. (19), the diving guidance objective shown in Eq. (10) can then be rewritten as

$$\begin{cases} \lim\limits_{t \to t_f} x_1(t) = \lim\limits_{t \to t_f} z_1(t) = 0 \\ \lim\limits_{t \to t_f} x_2(t) = \lim\limits_{t \to t_f} z_2(t) = 0 \end{cases} \tag{21}$$

Then the feedback control law of state space Eq. (20) is

$$\boldsymbol{v} = -\boldsymbol{k}\boldsymbol{z} \tag{22}$$

where $\boldsymbol{k} = [k_D, k_T]^T$ is the effective navigation ratio for which a value between 3 and 5 is frequently chosen in practice [13]. It is obvious that Eq. (22) is sufficient condition to Eq. (21), which means guidance objective can be achieved with the guidance law (22).

3.2. Maneuver control equations

Owing to the complicated outside aerodynamic force, gravity and the influence of zero LOS angle rate, the diving ballistic is much different from the two-body orbit of traditional ballistic missile in middle phase, so it is impossible to establish the maneuver control equations via the relative position and velocity directly. Guidance law (22) can steer vehicle to attack the ground fixed target with high precision, but the ballistic will be too straight to realize effective perception because of zero LOS angle rate. Considering that the guidance law (22) takes LOS angle and the varying rate as the main parameters to describe relative motion, the maneuver control equations construction will be much easier if the same parameters

are adopted. Therefore, in order to improve maneuver performance, we can add maneuver control law to Eq. (22):

$$\boldsymbol{v} = -\boldsymbol{kz} + \boldsymbol{u_m} \tag{23}$$

in which $\boldsymbol{u}_{\mathbf{m}} = [u_{mD}, u_{mT}]^T$ is the maneuver control law, so this novel control law can be then called integrated control law. With Eq. (23), it is very convenient to obtain different maneuver trajectories by designing maneuver control law $\boldsymbol{u}_{\mathbf{m}}$. The practical LOS angle rate can be expressed as follows by substituting Eq. (23) into state space Eq. (19):

$$\dot{\boldsymbol{z}} = -\boldsymbol{kz} + \boldsymbol{u}_{\mathbf{m}} \tag{24}$$

It can be seen from Eq. (24) that different maneuver forms can be obtained though modifying maneuver control law $\mathbf{u}_{\mathbf{m}}$. Substituting Eq. (23) into the inputs transform (17), the following can be obtained:

$$\begin{aligned}\boldsymbol{u} &= \boldsymbol{P}^{-1}(\boldsymbol{x})[-\boldsymbol{Q}(\boldsymbol{x}) + \boldsymbol{v}] \\ &= \frac{1}{(1/T_{go}^2) - A_{DT}^2}\begin{bmatrix} \frac{1}{T_{go}} & A_{DT} \\ -A_{DT} & -\frac{1}{T_{go}} \end{bmatrix} \\ &\quad \begin{bmatrix} -\left(\frac{\dot{v}}{v} + \frac{2}{T_{go}} + 1\right)\dot{\lambda}_D + A_{DT}x_2 - k_D x_1 + u_{mD} \\ -\left(\frac{\dot{v}}{v} + \frac{2}{T_{go}}\right)x_2 + A_{DT}\dot{\lambda}_D - k_T x_2 + u_{mT} \end{bmatrix}\end{aligned} \tag{25}$$

Eq. (25) shows that the diving guidance law which can realize high precision guidance and maneuvering flight is obtained by substituting the control law derived from feedback control and additional maneuver item into the original nonlinear equations. Based on the velocity azimuth rates studied above, the required control overload can be expressed as

$$\begin{cases} n_y = \dot{\gamma}_D v / g_0 \\ n_z = \dot{\gamma}_T v / g_0 \end{cases} \tag{26}$$

where n_y and n_z are the required longitudinal and lateral control overloads, respectively, g_0 is the gravity acceleration on the sea level. Then the total overload is

$$n_2 = \sqrt{n_y^2 + n_z^2} \tag{27}$$

The angle of attack can be obtained from (28) by inverse interpolation.

$$Y = C_L q S = g_0 n_2 \tag{28}$$

where Y is the aerodynamic lift, $q = \rho v^2/2$ is the dynamic pressure and the bank angle can be expressed as

$$\upsilon = \arctan(n_z/n_y) \tag{29}$$

4. Optimal maneuver strategy when encounter time is determined

It is clear that the diving maneuver penetration is the confrontation with air defense system. The defense system consists of detective radar and interceptor. Detective radar is adopted to measure and estimate the movement information of the vehicle and transit them to the ground-based defense system, which can be used to steer the interceptor to the target. As discussed in the above section, maneuvering flight form and the maneuver strategy play the key role in the improvement of interception capability effectively. However, we cannot make certain whether the vehicle acknowledges the movement information of interceptor, including the encounter time and the relative motion information. Then, the maneuver strategies with different conditions must be much different regardless of the same guidance laws and maneuver control equations. Consequently, we have to design the respective strategies when the encounter time is determined and undetermined. The guidance and maneuver logic can be expressed in Fig. 2.

Fig. 2 shows the complete guidance and maneuver logic. To begin with, as the basis of the further research of guidance law and maneuver strategy, it needs to establish the 3D nonlinear coupled relative motion equation based on terminal constraints and current motion states. Second, the nonlinear coupled motions equation will be decoupled into linear ones through feedback linearization, and the 3D guidance law which can satisfy multiple terminal constraints can be also obtained. Furthermore, it is easy to construct maneuver control equation by adding maneuver control item to the

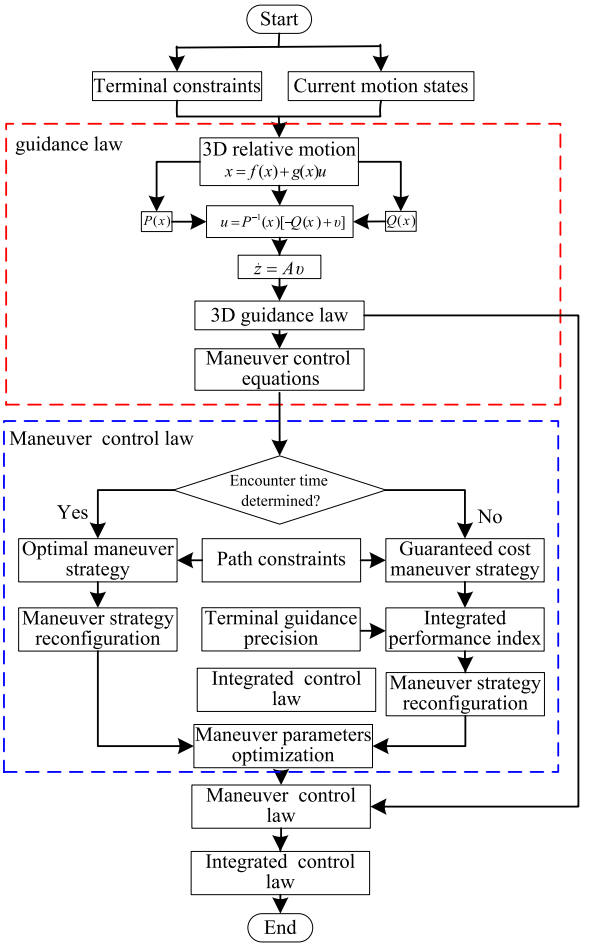

Fig. 2. Flow chart for the guidance and maneuver logic.

original guidance law. With this equation, it will establish the optimal performance indices to evaluate the maneuver performance and design the maneuver strategies using optimal control when the encounter time is determined and undetermined, respectively. In addition, considering the control capability limitation, especially the terminal guidance accuracy, the performance indices under different situations will be reconstructed, and then the optimal strategy and guaranteed cost maneuver strategy will be obtained as well.

This section will take full advantage of optimal control and parameter optimization to obtain diving optimal maneuver strategy with the determined encounter time.

4.1. Optimal maneuver strategy

Reasonable maneuver strategy is necessary for the effective penetration [13]. The penetration performance is closely related to the mutual flight velocities and overloads of evader and pursuer at encounter time. As the evader, penetration performance increases as velocity and overload increase. However, it is always unaccepted to maneuver blindly because of too much energy consumption or too small maneuver overload [13]; in other words, the penetration performance must be declined if maneuver strategy is designed unreasonable. Consequently, optimal control can be employed to resolve this problem.

To begin with, take longitudinal maneuver for example; the maneuver control equation can be rewritten as follows:

$$\begin{cases} \dot{x} = -k_D x + u_{mD} \\ y = x \end{cases} \tag{30}$$

where $x = z_1$ represents the longitudinal LOS angle rate. We can introduce optimal performance index based on energy consumption and LOS angle rate at encounter time:

$$J = \min\left[-\frac{1}{2}x^2(t_f) + \frac{1}{2}\int_0^{t_f} u_{mD}^2 \mathrm{d}t\right] \tag{31}$$

where t_f refers to the encounter time. The performance index (31) represents the minimum value of the sum of the maneuver energy consumption in the time interval $[0, t_f]$ and the maximum value of LOS angle rate at encounter time, which means we should design a control input u_{mD} to obtain maximum velocity and overload. With the performance index (31), the optimal control law of Eq. (30) can be given:

$$u_{mD}^* = -\boldsymbol{K}(t)x = -\boldsymbol{R}^{-1}\boldsymbol{B}^T\boldsymbol{P}(t)x \tag{32}$$

in which $\boldsymbol{B} = [1], \boldsymbol{F} = [-1], \boldsymbol{R} = [1]$, and $\boldsymbol{P}(t)$ can be calculated through differential Riccati Eq. [20]:

$$\begin{cases} \dot{\boldsymbol{P}}(t) + \boldsymbol{P}(t)\boldsymbol{A} + \boldsymbol{A}^T\boldsymbol{P}(t) - \boldsymbol{P}(t)\boldsymbol{B}\boldsymbol{R}^{-1}\boldsymbol{B}^T\boldsymbol{P}(t) = 0 \\ \boldsymbol{P}(t_f) = \boldsymbol{F} \end{cases} \tag{33}$$

The solution of Eq. (33) is

$$\boldsymbol{P}(t) = \frac{-2k_D\exp(-2k_D t_f)}{\exp(-2k_D t_f) + (2k_D - 1)\exp(-2k_D t)} \tag{34}$$

Different encounter times t_f (5–10 s), and effective navigation ratio $k_D = 4$ are set, the changing curve of optimal gain with time is expressed in Fig. 3.

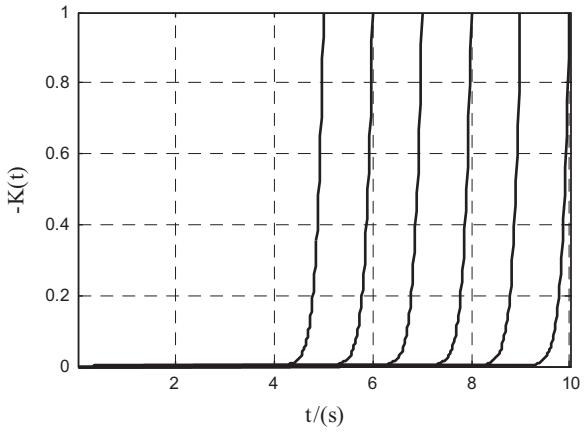

Fig. 3. $-\mathbf{K}(t)$ under different determined encounter times.

Fig. 3 illustrates that the maneuvering flight only occurs near the encounter time to save energy and increase the terminal overload as much as possible. Substituting Eq. (34) into Eq. (32), the optimal maneuver strategy can be computed:

$$u_{mD}^* = \frac{2k_D\exp(-2k_D t_f)}{\exp(-2k_D t_f) + (2k_D - 1)\exp(-2k_D t)}x \tag{35}$$

We can learn from the optimal guidance gain shown in Fig. 3 and Eq. (35) that it is unnecessary adopt any maneuvering flight when the relative distance between hypersonic vehicle and interceptor is large, and maneuver only occurs near the encounter time so that the energy can be saved and terminal overloads can be increased as much as possible. However, this strategy ignores the control capability limitation and the influence on terminal guidance accuracy caused by maneuvering flight, which means that the maneuver performance, control capability and guidance accuracy cannot be considered separately. In order to resolve this problem, we have to reconstruct the performance index and strategy based on the above analysis.

The performance index (31) is designed to get minimum energy consumption and maximum LOS angle rate at encounter time. It is clear that minimum energy consumption equals to maximum terminal velocity magnitude, and then we can reconstruct the index (31) as

$$J = \sup_{t = t_f}\left[k_{revise}x(t) + \frac{v(t)}{v_0}\right] \tag{36}$$

In Eq. (36), v_0 is the initial velocity; the velocity is normalized to let $v(t)/v_0 \in [0, 1]$. k_{revise} is the revise coefficient to make $k_{revise}x(t)$ have the same order of magnitude with $v(t)/v_0$. The performance index (36) is designed with the similar meaning with index (31) and the finite time H_∞ performance index [13], but it will be more effective because practical LOS angle rate and velocity are well considered. It is clear that the maneuver performance will be optimal when weighted average of the velocity magnitude and LOS angle rate at encounter time is the largest. With the novel performance index (36), combining maneuver performance, control capability and guidance

accuracy together, the new strategy can be designed:

$$u_{mD} = K_{Dmax}\exp\left(-\left(\frac{t-t_f}{\xi}\right)^2\right)x \tag{37}$$

where K_{Dmax} is the maximum maneuver amplitude, ξ can be employed to modify maneuver start and finish time. Being similar to the strategy shown in Eq. (35), a large amplitude maneuver near the encounter time is most effective, which can obtain larger overload and terminal velocity magnitude. Besides, another main advantage is that the maneuver amplitude will reduce to zero to ensure the terminal guidance accuracy, and the rate of control gain can also be modified by modulating the maneuver parameters K_{Dmax} and ξ. Consequently, compared with the strategy shown in Eq. (35), the maneuver control law (37) is more usable because the control capability and terminal guidance accuracy are fully considered, although it is the suboptimal maneuver strategy.

4.2. Simulation and parameters optimization

In the simulation of guidance performance testing, the 1976 U.S. Standard Atmosphere is used as the atmospheric model. Lockheed-Martin's CAV-H vehicle [1] whose weight is 907 kg, reference area is 0.4839 m^2 is employed. The equations of motion are integrated with a fourth-order Runge–Kutta method, and the altitude is treated as the stopping condition. The maneuver control parameters are $t_f = 60$ s, $\xi = 3$, and $k_{revise} = 180/\pi$. The initial and terminal parameters and path constraints are shown in Table 1.

The main simulation results for diving guidance and longitudinal maneuver are shown in Figs. 4–7. We can learn from the results that both the diving high precision and maneuvering flight can be realized with the aid of proposed strategy. All the terminal impact angle errors are smaller than 0.5°, LOS angle rates shrink down to zero at the end of diving flight, and additional overloads about 3–3.5 g were generated. In addition, all the movement states under different maximum maneuver amplitudes keep the same when the fight time is smaller than 55 s because the amplitudes are zero according to the maneuver strategy. When fight time is larger than 55 s, maneuvering flight starts, and the angles of attack shown in Fig. 4 increase rapidly to generate enough aerodynamic force to achieve large amplitude maneuver. However, as shown in Fig. 5, due to the maximum angle of attack and the rate of change limitation, the practical LOS angle rates and overloads cannot increase as required amplitude increases. Consequently, it can be seen from Figs. 6 and 7 that the difference between the trajectories with different

Table 1
Simulation parameters.

Initial velocity magnitude (v_0)	2000 m/s
Initial velocity slope angle (θ_0)	0°
Initial velocity azimuth (σ_0)	45°
Initial longitude (λ_0)	0°
Initial latitude (φ_0)	0°
Initial altitude (h_0)	40 km
Terminal longitude (λ_f)	1°
Terminal latitude (φ_f)	1°
Terminal velocity slope angle (θ_f)	−80°
Maximum angle of attack ($\alpha_{\max}$)	[−20°, 20°]
Maximum angle of attack rate ($\lvert\dot{\alpha}\rvert_{\max}$)	5° s^{-1}
Maximum overload ($N_{\max}$)	[0, 20g]
Maximum bank angle rate ($\lvert\dot{\nu}\rvert_{\max}$)	20° s^{-1}

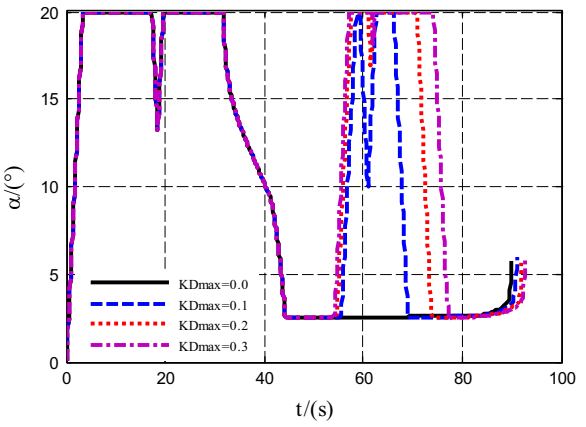

Fig. 4. Angle of attack versus time curves.

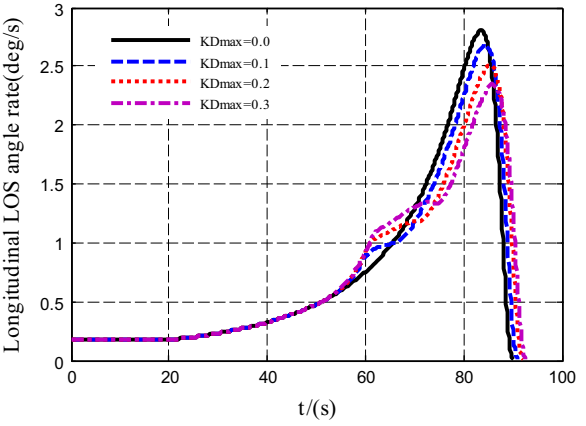

Fig. 5. Longitudinal LOS angle rate versus time curves.

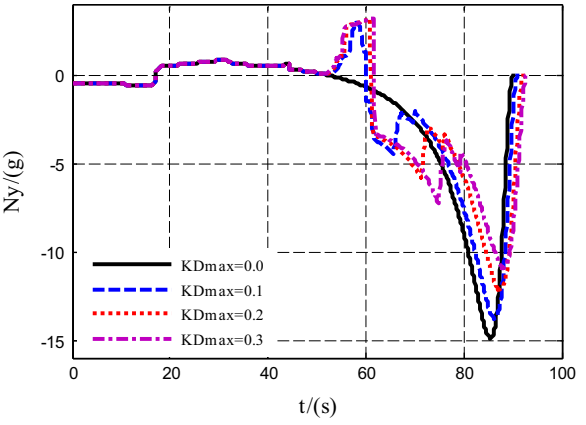

Fig. 6. Longitudinal overload versus time curves.

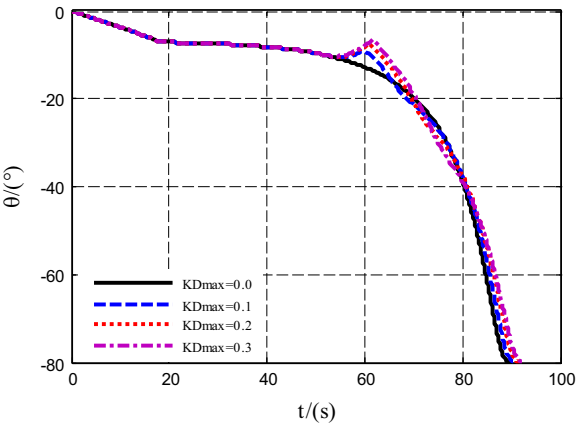

Fig. 7. Velocity slope angle versus time curves.

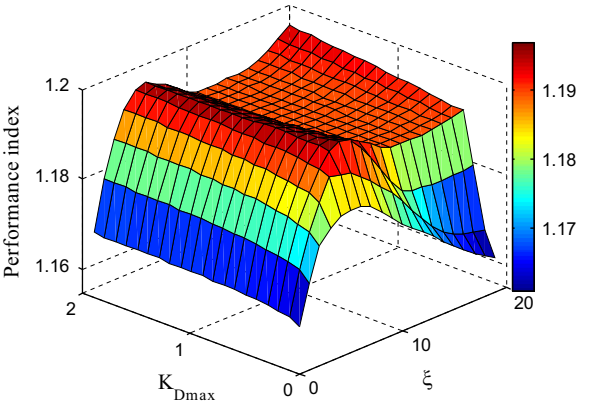

Fig. 8. Performance indices under different ξ and K_{Dmax}.

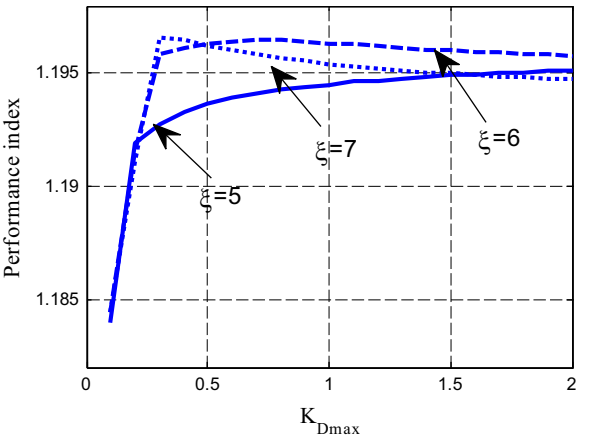

Fig. 9. Performance indices when $\xi = 5, 6, 7$.

maximum amplitudes is not so distinct, especially when $K_{Dmax} > 0.2$. Moreover, according to the maneuver strategy, the amplitude decreases as the flight time increases when $t > 60$ s so that the guidance accuracy can be ensured. In general, the proposed strategy is applicable to resolve the diving guidance problem.

It is known that maneuver performance can be influenced by maneuver amplitude and start time. Therefore simulation can only evaluate that the new proposed strategy is available for the guidance and maneuver tasks, but the performances under different parameters ξ and K_{Dmax} remain to be clarified. In order to obtain the optimal parameters, we set several different parameters $K_{Dmax} \in [0.1, 2.0], \xi \in [1, 20]$ under the same initial conditions for each case, and the simulation results are shown in Figs. 8 and 9. The results demonstrate that the performance index is closely related to ξ and K_{Dmax}; both of them cannot be selected too small or too large because of too much energy consumption or too small LOS angle rate. Combining the results in Figs. 8 and 9, it can be concluded that the maneuver performance will be optimal when ξ is selected near six. In addition, or each given ξ, the index increases rapidly as the parameter K_{Dmax} increases when it is smaller than 0.3. However, due to the maximum angle of attack and the rate of change, the maneuver performance cannot be further improved when K_{Dmax} is larger than 0.5. As a result, we can obtain elementary conclusion that the maneuver performance will reach to the best when $\xi = 6$, and K_{Dmax} is larger than 0.3.

The above simulation aims to achieve maneuvering flight, ignoring the influence on terminal guidance accuracy. The indices and terminal guidance accuracies under different maneuver parameters ξ and K_{Dmax}, including miss distance and impact angle, are shown in Table 2. Firstly, compared with the un-maneuverable trajectory with the index 1.152, the maneuver performance can be much improved by maneuvering flight. Secondly, setting a relative small values of K_{Dmax} and ξ can achieve a highly precise guidance, otherwise both the maneuver performance and guidance accuracy will be degraded, especially for the terminal accuracy Moreover, as a complementarily for the above simulation, $\xi = 6$ and $K_{Dmax} = 0.4$ are the expected optimal maneuver parameters owing to the dramatic increase of miss distance and impact angle error increase dramatically with a K_{Dmax} larger than 0.6.

Table 2
Guidance accuracy and performance index under different ξ and K_{Dmax}.

K_{Dmax}	ξ	J	Miss distance (m)	Impact angle (deg)
0	—	1.152	1.652	−80.097
0.2	2	1.174	1.681	−79.873
0.2	4	1.187	1.124	−79.933
0.2	6	1.192	1.702	−80.203
0.2	8	1.185	2.221	−79.662
0.4	2	1.176	1.362	−79.908
0.4	4	1.189	1.743	−79.731
0.4	6	1.196	1.876	−80.809
0.4	8	1.194	56.21	−82.330
0.6	2	1.176	1.142	−79.772
0.6	4	1.190	1.798	−80.126
0.6	6	1.196	143.5	−86.413
0.6	8	1.194	416.7	−87.979

5. Optimal maneuver strategy when encounter time is undetermined

However, as for the hypersonic vehicle which is regarded as an evader, the design of maneuver strategy will be much more difficult if interceptor's movement information, such as the encounter time, cannot be determined perfectly. Guaranteed cost maneuver strategy which needs maneuvering flight to be carried out all over the dive phase can be adopted to resolve this problem. Be similar to the above optimal strategy, optimal control will be employed to design the maneuver strategy here, terminal guidance accuracy and control capability will be fully considered, and the corresponding parameters will be also optimized.

5.1. Guaranteed cost maneuver strategy

Taking longitudinal maneuver for example, in order to obtain the guaranteed cost maneuver strategy based on optimal control, we should introduce optimal performance index at first:

$$J=\min\left[\frac{1}{2}x(T_g)\mathbf{F}x(T_g)+\frac{1}{2}\int_0^{T_g}u_{mD}^2-x^2\,\mathrm{d}t\right] \tag{38}$$

where T_g is the flight time-to-go. The performance index (38) is constructed to obtain minimum energy consumption and maximum LOS angle rate during the whole dive phase, and let terminal LOS angle rate equal to the required one. With the state space Eq. (30) and performance index (38), the key step of obtaining optimal control law is the solution of differential *Riccati* Eq. [20]:

$$\begin{cases}\dot{\boldsymbol{P}}(t)+\boldsymbol{P}(t)\boldsymbol{A}+\boldsymbol{A}^T\boldsymbol{P}(t)-\boldsymbol{P}(t)\boldsymbol{B}\boldsymbol{R}^{-1}\boldsymbol{B}^T\boldsymbol{P}(t)+\boldsymbol{Q}(t)=0\\ \boldsymbol{P}(t_f)=\boldsymbol{F}\end{cases} \tag{39}$$

where $\boldsymbol{A}=[-k_D],\boldsymbol{B}=[1],\boldsymbol{R}=[1],\boldsymbol{Q}=[-1],\boldsymbol{F}=[0]$, the solution of Eq. (39) is

$$\boldsymbol{P}(t)=-k_D+\sqrt{k_D^2-1}\cdot\tanh\left((T_g-t)\sqrt{k_D^2-1}+\operatorname{atanh}\left(\frac{k_D}{\sqrt{k_D^2-1}}\right)\right) \tag{40}$$

substituting $\boldsymbol{P}(t)$ into optimal control law, the maneuver strategy can be obtained.

$$u_{mD}^*=-\boldsymbol{K}(t)x=\left(k_D-\sqrt{k_D^2-1}\cdot\tanh\left((T_g-t)\sqrt{k_D^2-1}+\operatorname{atanh}\left(\frac{k_D}{\sqrt{k_D^2-1}}\right)\right)\right)x \tag{41}$$

Different guidance finish time T_g(50–100 s), and effective navigation ratio $k_D=4$ are set; the changing curve with time is expressed in Fig. 10.

As shown in Fig. 10, we can learn that the maneuvering flight should be carried out during the whole flight process to ensure the maneuver performance, and maneuver control gain will reduce to zero rapidly to decrease the influence on terminal guidance accuracy as much as possible. However, this strategy can only improve maneuver performance by increasing the terminal velocity instead of LOS angle rate because of the constant maneuver gain, ignoring the control capability limitation and the path constraints resulting from the too large rate of the control gain in the end of dive phase. Consequently, we have to reconstruct the performance index and the theoretical optimal maneuver strategy.

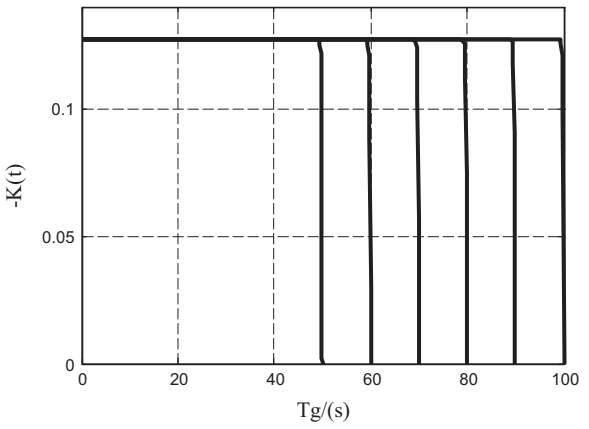

Fig. 10. $-\mathbf{K}(t)$ under different terminal times.

Maneuver performance is closely related to the flight velocity and overload, which means that with the larger the velocity and overload, the better the maneuver performance. Therefore, for similar performance index (38), we can reconstruct the performance index which consists of the terminal velocity magnitude and the LOS angle rate integration during the whole dive phase to make it more usable in practice. Here, the LOS angle rate integration is employed to describe the overload magnitude.

$$J_1=\sup\left[k_v\frac{v(T_g)}{v_0}+k_{\dot\lambda}\int_0^{T_g}\dot\lambda_D^2\mathrm{d}t\right] \tag{42}$$

in which v_0 and $v(T_g)$ are the initial and practical terminal velocities, respectively, and $k_v,k_{\dot\lambda}$ are the revise coefficients. This performance is designed to obtain maximum terminal velocity and overload which can be increased by maneuvering flight. However, it is known that maneuvering flight can cause serious influence to terminal guidance accuracy, and even lose the target if the amplitude is designed too large. Consequently, based on the novel constructed index (42), it is better to construct the integrated performance index combining terminal guidance accuracy together.

$$J_2=\sup\left[k_v\frac{v(T_g)}{v_0}+k_{\dot\lambda}\int_0^{T_g}\dot\lambda_D^2\mathrm{d}t-k_{Er}Er-k_\theta|\theta(T_g)-\theta_f|\right] \tag{43}$$

where Er represents terminal miss distance, $\theta(T_g)$ is the practical terminal velocity slope angle, both k_{Er} and k_θ are the corresponding revise coefficients. Compared with the index which only aims to obtain minimum energy consumption and maximum predict error described in Ref. [13], this index is more usable because both the maneuver performance and guidance accuracy are fully considered. This index shows that the larger the terminal velocity and $\int_0^{T_g}\dot\lambda_D^2\,\mathrm{d}t$, the better the integrated performance. By contrast, the smaller the terminal impact errors, the better the integrated performance. As a result, we have

to design the maneuver strategy to improve maneuver performance and ensure guidance accuracy.

In order to increase the reconstructed performance index (43) as much as possible, it is necessary to reconstruct the maneuver strategy further. Great many maneuver models can be well employed to enhance maneuver performance, such as constant acceleration model, Singer model and sinusoid model which can be also called weave model, in which the last one is the most effective commonly [18]. Weaving maneuver has already been adopted to improve maneuver performance for anti-ship missile successfully [21], but it cannot be employed to achieve maneuver for hypersonic vehicle in dive phase directly because of the serious influence on the terminal guidance accuracy. Therefore, in order to take full advantage of the excellent performance of weaving maneuver and decrease the influence on the guidance accuracy at the same time, which means generate flexible trajectory and enhance maneuver performance, we should redesign the maneuver strategy based on the weaving trajectory proposed in Refs. [18,21].

$$u_{mD}=\begin{cases} K_{Dmax}\ \sin\left(F_D\frac{h_0-h}{h_0-h_{midd}}\pi\right) & h>h_{midd} \\ 0 & h<h_{midd} \end{cases} \tag{44}$$

where K_{Dmax} and F_D are the maneuver amplitude and frequency, respectively, h is the practical altitude and h_{midd} is the finish altitude of maneuver. The reconstructed maneuver strategy can be explained as weaving maneuver will be adopted to enhance the maneuver performance when $h>h_{midd}$, and the maneuver amplitude keeps constant zero if $h<h_{midd}$ to ensure the terminal guidance accuracy. In this way, the maneuver performance can be improved with the weave maneuver model, and the guidance accuracy can also be ensured because of the zero maneuver amplitude when $h<h_{midd}$. Like the optimal strategy with determined encounter time, this strategy is the suboptimal solution of the guaranteed cost maneuver strategy, but it will be more useful because the terminal guidance accuracy is also fully considered. Besides, different maneuver trajectories can also be obtained through modifying the control parameters.

5.2. Simulation and parameters optimization

The same initial and terminal simulation parameters introduced in Section 4.2 are taken, and CAV-H model is also employed in the simulation. The main simulation results with the maneuver parameters $F_D=4$, $h_{midd}=5$ km, $k_v=1$, $k_\lambda=180/\pi$,$k_{Er}=0.01$ and $k_\theta=1$ are shown in Figs. 11–14. It can be seen from the results that the novel proposed 3D guidance law and guaranteed cost maneuver strategy can steer the vehicle to attack the target with the required angle even if large amplitude maneuvering flights are adopted when $h_{midd}>5$ km. The terminal miss distances and impact angle errors are smaller than 2 m and 1°, respectively. The maneuver trajectories including angle of attacks are much different from the trajectories without maneuver and they will be more flexible when the amplitude gets larger. During the whole dive phase, there are great many collapses for the LOS angle rates shown in Fig. 12, overloads expressed in Fig. 13 and velocity slope angles depicted in Fig. 14, but the terminal guidance accuracy can be ensured because of the zero maneuver amplitude at the end of flight. However, due to the maximum angle of attack and the limited rate of change,

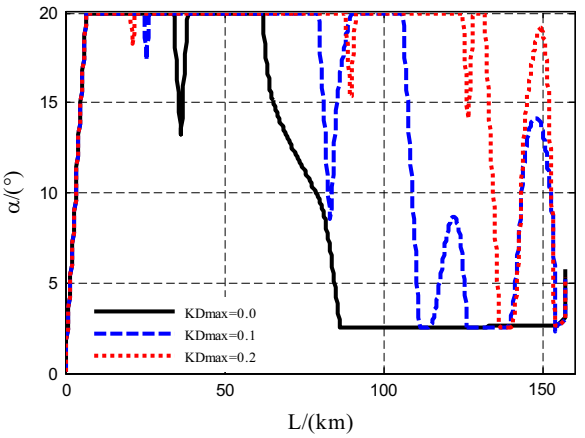

Fig. 11. Angle of attack versus range curves.

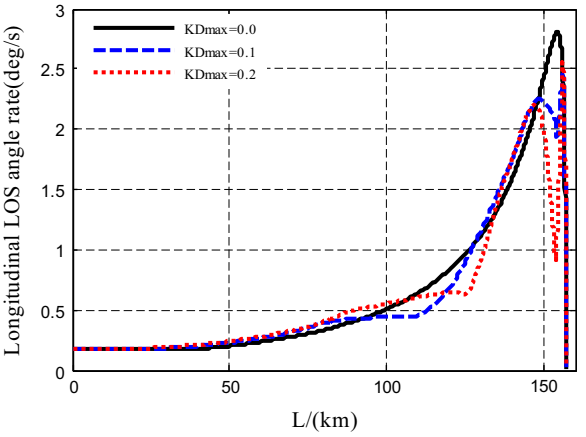

Fig. 12. Longitudinal LOS angle rate versus range curves.

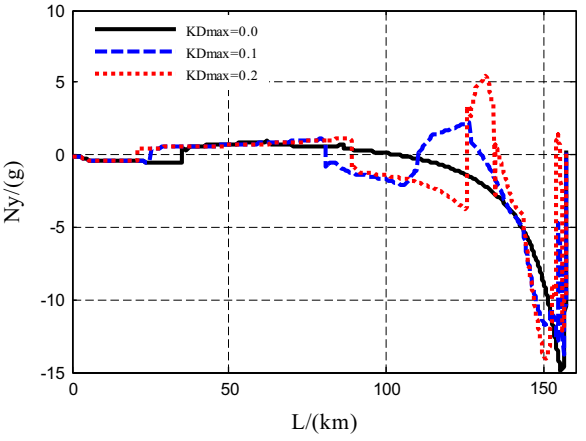

Fig. 13. Longitudinal overload versus range curves.

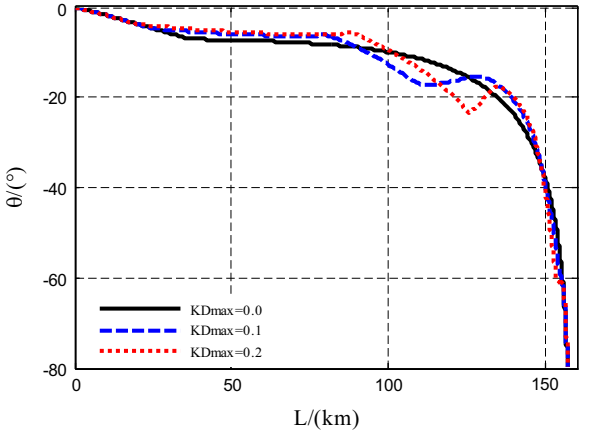

Fig. 14. Velocity slope angle versus range curves.

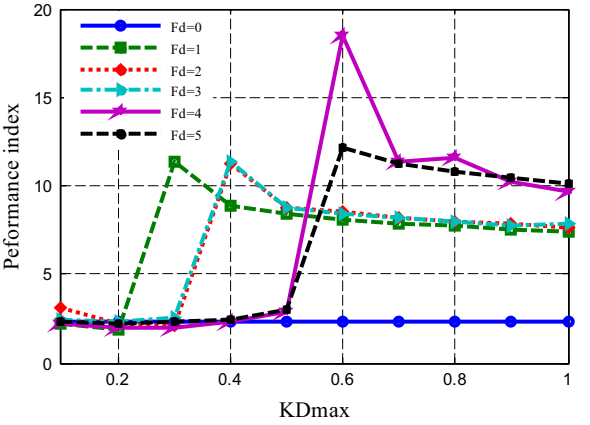

Fig. 15. Maneuver performance indices.

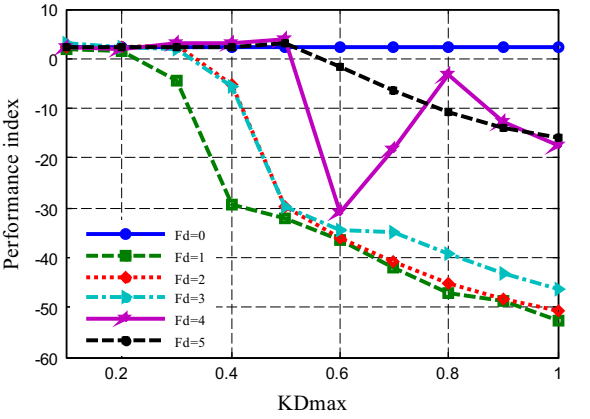

Fig. 16. Integrated performance indices.

the practical maneuver ranges cannot increase as the maneuver amplitudes increase. These simulation results indicate the practicability of the 3D guidance law and the proposed guaranteed cost maneuver strategy.

The above simulation can only confirm the guaranteed cost maneuver strategy can accomplish high precision guidance as well as maneuvering flight at the same time, but the maneuver performance under different parameters still needs to be validated. In order to test the maneuver performance under different maneuver frequencies and amplitudes and obtain the optimal guaranteed cost maneuver strategy, we set several different maneuver parameters under the same initial condition, including $K_{Dmax}=$ 0–1 and $F_D=0$–5. The maneuver performance indices and integrated performance indices are shown in Figs. 15 and 16, respectively.

Fig. 15 shows that the maneuver performance which is closely related to the amplitude and frequency which can be enhanced by maneuvering flight effectively. For each given frequency ($K_{D\,\max}\neq 0$), the amplitude of maneuver performance increases initially and decreases afterwards to a nearly same value due to the large energy consumption. The peak values of maneuver performance are much different from each other for different given frequencies. Additionally, it indicates that the smaller the maneuver frequency is, the better the maneuver performance can be achieved when the amplitude is less than 0.6. The main reason is that the maneuver range and the LOS angle rate in each maneuver period increase as the frequency decreases when the amplitude is small. However, the performance with different frequencies tends to decrease when the amplitude is above 0.6 because of the large energy consumption and control capability limitation. Consequently, reasonable maneuver frequency and amplitude are necessary to improve the maneuver performance.

Fig. 16 and Table 3 illustrate that the integrated performance indices are much different when the terminal guidance accuracy is fully considered, and maneuvering flight can exert a serious influence on the terminal guidance accuracy, especially for large amplitude maneuver. Owing to the improvement of maneuver performance and relative high guidance accuracy, the integrated performance index under each given maneuver frequency ($K_{D\,\max}\neq 0$) increases initially with increasing amplitude. But the index turns to decrease if the amplitude continues increasing because of the decline of guidance accuracy caused by large amplitude maneuver. Moreover, for the given amplitude, the larger the maneuver frequency is, the better the integrated performance index can be achieved, especially for relatively small amplitude. The main reason

Table 3
Guidance accuracy and performance index under different K_{Dmax} and F_D.

K_{Dmax}	F_D	J_1	J_2	Miss distance (m)	Impact angle (deg)
0	–	2.529	2.429	1.648	−80.096
0.2	2	1.858	1.561	1.062	−80.295
0.2	4	1.985	1.592	1.808	−80.391
0.2	6	1.992	1.980	1.575	−80.009
0.4	2	11.34	−5.494	283.2	−88.273
0.4	4	2.213	1.996	1.428	−80.216
0.4	6	4.201	4.159	1.282	−79.959
0.6	2	8.131	−37.203	403.7	−83.127
0.6	4	17.15	−30.15	98.66	79.904
0.6	6	2.916	2.849	1.240	−79.936
0.8	2	7.690	−45.824	797.6	−81.919
0.8	4	11.700	−3.700	31.74	−84.593
0.8	6	12.297	−1.063	38.07	−84.485

is that the maneuver range and the errors in each period caused by maneuvering flight, including position and direction errors, will be enlarged when the frequency is small. It is these errors which cannot be eliminated by the limited control capability that leads to the decline of the terminal guidance precision and performance index. In addition, the guidance accuracy and integrated index will continue declining as the amplitude increases.

The simulation results for the two different performance indices are compared; we can learn that contradiction exists between high precision guidance and maneuvering flight. For example, the maneuver performance is the optimal when $K_{Dmax}=0.6, F_D=4$, but integrated performance is decreased so much because of the too large impact errors. Therefore, both the maneuver frequency and amplitude cannot be selected too large or too small no matter whether terminal guidance accuracy is considered.

6. Conclusions

This study presents a novel diving maneuver strategy considering terminal guidance accuracy for hypersonic vehicles. The main characteristic of the proposed methodology lies in the fact that it takes full advantage of three-dimensional diving movement, optimal control and parameter optimization to realize high precision guidance and obtain optimal maneuver strategy at the same time. In addition, considering the control capability limitation, the performance indices and maneuver strategies are reconstructed when the encounter time is determined and undetermined. The major advantages of the proposed algorithm can be listed as follows:

1) The three-dimensional nonlinear relative coupled motion equations are constructed without any assumptions and approximations, which means the coupling characteristic is fully materialized in the equations.
2) Both the feedback linearization and feedback control are adapted so that the solution of the guidance problem is greatly simplified, and the maneuver control equations are obtained based on the diving guidance law.
3) It makes best use of optimal control to obtain the maneuver strategies, and reconstructs the performance indices and strategies considering terminal guidance accuracy and control capability. All the maneuver control parameters are optimized by simulation experiment.
4) It can be concluded that the maneuvering flight near the encounter time is the most effective strategy. The guaranteed cost maneuver strategy is necessary when the encounter time is undetermined, and both the maneuver frequency and amplitude cannot be selected too small or large.

However, there are also some disadvantages, in which the maneuver control parameters optimization is the main research topic for further study. In general, the proposed algorithm can provide some reference for the diving guidance of an RLV, hypersonic vehicle, etc.

Acknowledgments

This work was supported by the National Natural Science Foundation of China (61104200) and the National University of Defense Technology Innovation Foundation for Postgraduates (B140103).

References

[1] Phillips T.H. A common aero vehicle (CAV) model, description and employment guide, Schafer Corporation for AFRL and AFSPC, 27 January 2003.
[2] George R. The common aero vehicle; space delivery system of future, AIAA paper 1999–4425, August, 1999.
[3] Lu P. Stephen F., Morgan B., Gliding guidance of high L/D hypersonic vehicles. AIAA paper 2013–4648, August, 2013.
[4] Lu P., Frank R.C., Nonlinear optimal guidance. AIAA paper 2006–6079, August, 2006.
[5] K.J. Chen, H.Y. Zhao, An optimal guidance law of maneuvering reentry vehicle at tacking ground fixed target, J. Astronaut. 15 (1) (1994) 1–7. (in Chinese).
[6] P. Wu, M. Yang, Integrated guidance and control design for missile with terminal impact angle constraint based on sliding mode control, J. Syst. Eng. Electron. 21 (4) (2010) 623–628.
[7] T. Shima, J. Shinar, H. Weiss, New interceptor guidance law integrating time-varying and estimation delay models, J. Guid. Control Dyn. 26 (2) (2003) 295–303.
[8] Fabio A. de Almeida Improving maneuver performance in unmanned aerial vehicles through learning-based reference management. AIAA paper AIAA-2013–4616, August, 2013.
[9] B. Jarmark, A.W. Merz, J. Breakwell, The variable speed tail-chase aerial combat problem,, J. Guid. Control Dyn. 4 (3) (1981) 323–328.
[10] T. Shima, J. Shinar, Time-varying linear pursuit–evasion game models with bounded controls, J. Guid. Control Dyn. 25 (3) (2002) 425–432.
[11] G.M. Anderson, Comparison of optimal control and different ialgame intercept guidance laws, J. Guid. Control Dyn. 4 (2) (1981) 109–115.
[12] J. Shinar, S. Gutman, Three-dimensional optimal pursuit and evasion with bounded controls, IEEE Trans. Autom. Control 25 (3) (1980) 492–496.
[13] Y. Guo, Y. Yao, S.C. Wang, Maneuver control strategies to maximize prediction errors in ballistic middle phase, J. Guid. Control Dyn. 36 (4) (2013) 1225–1234.
[14] Guo Y., Wang S.C., Yao Y. Maneuver strategy of evader considering detection system. AIAA paper 2011–6713, August, 2011.
[15] D. Dionne, H. Michalska, J. Shinar, Decision-directed adaptive estimation and guidance for an interception endgame, J. Guid. Control Dyn. 29 (4) (2006) 970–980.
[16] J. Shinar, V. Turetsky, Y. Oshman, Integrated estimation guidance design approach for improved homing against randomly maneuvering target, J. Guid. Control Dyn. 30 (1) (2007) 154–161.
[17] E.J. Ohlmeyer, Root-mean-square miss distance of proportional navigation missile against sinusoidal target, J. Guid. Control Dyn. 19 (3) (1996) 563–568.
[18] P. Zarchan, Proportional navigation and weaving targets, J. Guid. Control Dyn. 18 (5) (1995) 969–974.
[19] A. Isidori, Nonlinear Controql Systems, Bertelsmann Springer Publishing Group, London, 2005.
[20] U. Shaked, V. Suplin, A new bounded real lemma representation for the continuous-time case, IEEE Trans. Autom. Control 46 (9) (2001) 1420–1426.
[21] Yoon-Hwan K., Min-Jea T., Guidance synthesis for evasive maneuver of anti-ship missiles, AIAA paper 2007–6783, August, 2007.